Solid State Spin-Wave Quantum Memory for Time-Bin Qubits

Mustafa Gündoğan,[1] Patrick M. Ledingham,[1,*] Kutlu Kutluer,[1] Margherita Mazzera,[1,†] and Hugues de Riedmatten[1,2]
[1]*ICFO-Institut de Ciencies Fotoniques, Mediterranean Technology Park, 08860 Castelldefels (Barcelona), Spain*
[2]*ICREA-Institució Catalana de Recerca i Estudis Avançats, 08015 Barcelona, Spain*
(Received 13 January 2015; revised manuscript received 25 February 2015; published 12 June 2015)

We demonstrate the first solid-state spin-wave optical quantum memory with on-demand read-out. Using the full atomic frequency comb scheme in a $Pr^{3+}:Y_2SiO_5$ crystal, we store weak coherent pulses at the single-photon level with a signal-to-noise ratio > 10. Narrow-band spectral filtering based on spectral hole burning in a second $Pr^{3+}:Y_2SiO_5$ crystal is used to filter out the excess noise created by control pulses to reach an unconditional noise level of $(2.0 \pm 0.3) \times 10^{-3}$ photons per pulse. We also report spin-wave storage of photonic time-bin qubits with conditional fidelities higher than achievable by a measure and prepare strategy, demonstrating that the spin-wave memory operates in the quantum regime. This makes our device the first demonstration of a quantum memory for time-bin qubits, with on-demand read-out of the stored quantum information. These results represent an important step for the use of solid-state quantum memories in scalable quantum networks.

DOI: 10.1103/PhysRevLett.114.230501 PACS numbers: 03.67.Hk, 42.50.Ex, 42.50.Gy, 78.55.Qr

Photonic quantum memories are essential in quantum information science (QIS) where they are used as quantum interfaces between flying and stationary qubits. They enable the synchronization of probabilistic quantum processes, e.g., in quantum communication [1,2] and computing [3]. The implementation of quantum memories (QMs) for light requires strong interactions between individual photons and matter. This can be achieved by placing individual quantum systems (e.g., single atoms) in high finesse cavities [4] or by using ensembles of atoms, where the photons are mapped onto collective atomic excitations. Atomic systems are natural candidates as QMs [5–14], but solid state systems offer interesting perspectives for scalability and integration into existing technology [15–21].

Rare-earth ion doped solids are promising candidates for high performance solid state QMs since they have excellent coherence properties at cryogenic temperatures [22]. They also exhibit large static inhomogeneous broadening of the optical transitions, which can be tailored and used as a resource for various storage protocols, e.g., enabling temporally [23] and spectrally [24] multiplexed quantum memories. Recent experimental progress includes qubit storage [15,24–27], highly efficient quantum storage of weak coherent states [16], storage of entangled and single photons [17,18,28], entanglement between two crystals [29], and quantum teleportation [30].

Yet, nonclassical states have so far only been stored as collective optical atomic excitations with fixed storage times [17,18,28]. While this may provide a useful resource if combined with massive multiplexing and deterministic quantum light sources [24], the ability to read-out the stored state on demand is essential for applications where the quantum memory is used as a synchronizing device. On-demand read-out can be achieved by actively controlling the optical collective excitations [16], with a storage time limited by the coherence of excited states. Another solution is to transfer the optical excitations to long-lived collective spin excitations (or spin waves), using strong control pulses [31–33]. This gives access to much longer storage times [34,35]. Operating a solid state spin-wave memory in the quantum regime has so far remained elusive, because of an insufficient signal-to-noise ratio (SNR) at the single-photon level [33].

Here, using the full atomic frequency comb (AFC) protocol in a $Pr^{3+}:Y_2SiO_5$ crystal we store and retrieve weak coherent pulses on demand with a SNR > 10 for single-photon-level input. Using a narrow-band filter based on spectral hole burning in a second crystal, we achieve an unconditional noise floor of $(2.0 \pm 0.3) \times 10^{-3}$ photons per pulse. The use of spectral holes as narrow-band filters has been already demonstrated in storage schemes operating in a classical fashion [36–38], but it is here exploited for the first time to enter the quantum regime. Finally, we demonstrate storage and retrieval conditional fidelities (i.e., assuming that a photon was reemitted) higher than classical memories for time-bin qubits at the single-photon level, taking into account the Poissonian statistics and the finite efficiency of the memory. These results represent the first demonstration of a solid state spin-wave quantum memory, enabling on-demand read-out of the stored qubits. They also provide the first example of a spin-wave quantum memory for time-bin qubits (for any system), an essential resource in quantum communication [39] and processing [40].

The AFC technique [15,23] is based on spectral tailoring of an inhomogeously broadened absorption line into a comb-shaped structure with periodicity Δ. The input pulses resonant with the comb are mapped onto a collective optical atomic excitation. After an initial dephasing, the excitations

rephase at a time $1/\Delta$ giving rise to a forward collective emission [15,23]. Before the coherent emission two strong control pulses are applied to transfer the excitation to and from a long-lived ground state to achieve the spin-wave storage of the input pulses. The full AFC scheme requires ions with at least three ground states, one being used as an auxiliary state for optical pumping [41]. The spin-wave storage efficiency is given by $\eta_{\mathrm{SW}} = \eta_{\mathrm{AFC}} \times \eta_T^2 \times \eta_C$, where η_{AFC} is the efficiency of the storage at the excited state and depends on the optical depth and comb finesse [23], η_C accounts for the decoherence during the ground state storage, and η_T is the transfer efficiency of the control pulses.

The realization of the full AFC scheme in the single-photon regime is challenging as the strong control pulses create noise that may dominate the weak signal retrieved from the memory. Two main mechanisms are responsible for this noise: (i) spatial leakage from the control mode into the input mode due to scattering from the optical surfaces and (ii) interaction of the control pulses with residual population in the spin storage state due to imperfect optical pumping. The latter includes collective effects, such as free-induction decay, or incoherent fluorescent emission. Note that four-wave mixing is not a dominant source of noise in our system, in contrast to Raman memories in atomic vapors [45] (see Ref. [41] for details). To reduce the noise we employ spatial, temporal, and spectral filtering. The spectral filtering is challenging in $Pr^{3+}:Y_2SiO_5$, as the input and control frequencies are separated by only 10.2 MHz [see Fig. 1(b)]. As a narrow-band spectral filter we use a second $Pr^{3+}:Y_2SiO_5$ crystal where we prepare spectral holes of variable width [36–38].

The experimental arrangement and the relevant energy level scheme of Pr^{3+} at 606 nm are shown in Fig. 1. The main laser beam at 606 nm (Toptica TA-SHG pro) is split into three to be used as the input mode, the filter preparation mode, and lastly for the control pulses and memory preparation. They all pass through acousto-optical modulators (AOMs) in a double-pass configuration, driven by an arbitrary waveform generator (Signadyne), to create the necessary pulse sequences. The beams are then carried with polarization-maintaining single-mode optical fibers to another optical table where the cryostat is located. The maximum available optical powers are about 20 mW, 3.5 mW, and 150 μW for the control, filter preparation, and input modes, respectively, measured in front of the cryostat. The frequency of the 606 nm laser is stabilized by the Pound-Drever-Hall technique to a homemade temperature controlled Fabry-Perot cavity housed in a vacuum chamber. The input light is linearly polarized close to the optical D_2 axis to maximize the interaction with the Pr^{3+} ions. The measured optical depth of the Pr^{3+} transition at 606 nm is about 7 for both the memory and filter crystal. In both cases, the inhomogeneous linewidth is about 6 GHz. After the storage, the retrieved signal passes through different diffraction order modes (−1st and 1st) of two consecutive AOMs, acting as a temporal gate before

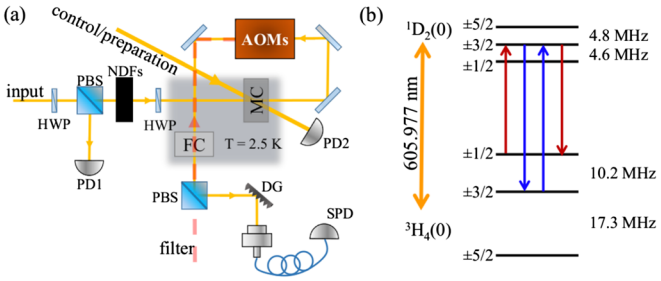

FIG. 1 (color online). (a) Quantum memory setup. The memory (MC) and filter (FC) crystals are located inside a liquid-free cooler (Oxford V14) operating at a temperature of 2.5 K. They are both 3 mm long and doped with a Pr^{3+} concentration of 0.05%. The control and input beams are steered towards the memory with an angle of ∼1.5°, leading to leading to an extinction ratio of 10^{-5}. The beam diameters on the crystal are 280 and 90 μm for strong and input modes, respectively. The weak coherent states are prepared by attenuating bright pulses with variable neutral density filters (NDFs). A portion of the input beam is picked up before the NDF and sent to a photodiode (PD1) for the calibration of the mean photon number per pulse. A mechanical shutter is used to protect the single-photon detector (SPD) during the memory and filter preparation. HWP: half-wave plate. AOM: acousto-optical modulator. DG: diffraction grating. The dashed red beam indicates the filter preparation mode. (b) Hyperfine splitting of the first sublevels of the ground $^3H_4$ and the excited $^1D_2$ manifold of Pr^{3+} in Y_2SiO_5.

passing through the filter crystal. A diffraction grating DG is then used to filter the noise not resonant with the crystal. The retrieved signal is coupled with 60% efficiency into a single-mode fiber for connection to the single photon detector (SPD, PicoQuant τ SPAD-20, detection efficiency $\eta_d = 60\%$, dark count rate ∼10 Hz). The total transmission of the input beam from the cryostat to the SPD is about 13%.

We tailor the AFC using optical pumping techniques as described in Refs. [33,46]. We isolate a single class of atoms [47,48] and create a 3.5 MHz wide AFC with $\Delta =$ 200 kHz on the $1/2_g - 3/2_e$ transition within a 14 MHz wide transparency window (see Ref. [41] for details and for a comb example). During the preparation of the memory, the population removed from the comb is stored in the auxiliary $5/2_g$ state, while the $3/2_g$ state is emptied. To further remove unwanted residual population in the $3/2_g$ state, we apply an extra series of 100 pulses on the $3/2_e - 3/2_g$ transition after the comb preparation. We then start the single-photon-level storage measurements. Weak Gaussian input pulses with a full width at half maximum (FWHM) duration of 430 ns and mean photon number μ_{in} are mapped on the AFC and transferred to spin waves thanks to a strong control pulse. The control pulses have a Gaussian temporal profile with a FWHM of 700 ns and are spectrally chirped by 5 MHz about the $3/2_e - 3/2_g$ transition. For each comb preparation, 1000 storage trials are performed with a repetition rate of ∼7 kHz. The full cycle has a period of 700 ms, including memory preparation and light storage. It is synchronized with the cryostat cycle to reduce the

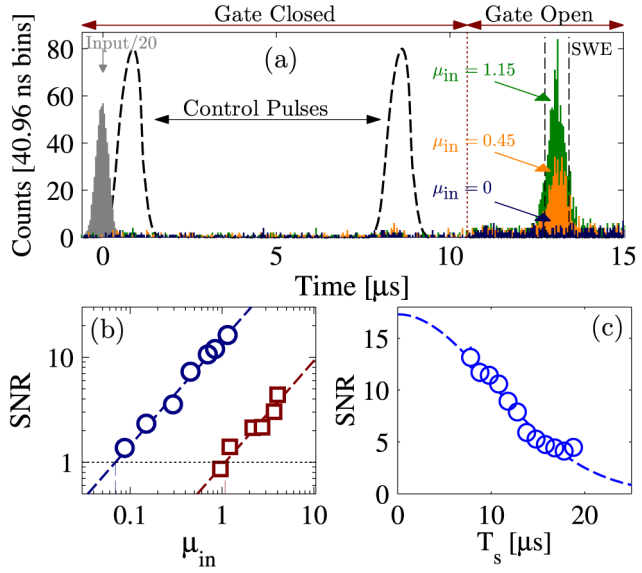

FIG. 2 (color online). (a) Time histograms of the retrieved photons measured for different input photon numbers when a transparency window 2 MHz wide is prepared in the filter crystal. The input ($\mu_{in} = 0.9$) and the control pulses, as measured in photon counting and from a reference photodiode (PD2 in Fig. 1), respectively, are also displayed. The chosen 0.7 μs wide detection window is indicated by the dashed lines about the three-level echo; it includes ~80% of the counts in the full echo mode. (b) Signal-to-noise ratio (SNR) as a function of the number of input photons for different filter widths. Circles: 2 MHz. Squares: 14 MHz. The error bars (smaller than the data points) are evaluated with Poissonian statistics. The black dotted line indicates the limit of detection SNR = 1. The dashed lines are linear fits of the experimental data. (c) Decay of the SNR as a function of the spin-wave storage time T_S with average photon number $\mu_{in} = 1$. From the fit with a Gaussian profile, the spin inhomogeneous broadening $\gamma_{in} = (26 \pm 1)$ kHz can be extrapolated. By comparing the SNR that we measure at a storage time $T_S = 7.8$ μs with the extrapolation at $T_S = 0$ μs, we can evaluate the decoherence term η_C to be about 75%.

effect of vibrations. The sequence is then repeated 500 to 1000 times to accumulate sufficient statistics.

Figure 2(a) shows the time histograms of the retrieved photons with different μ_{in}. For this measurement, the crystal filter has a hole width of 2 MHz. The spin-wave storage time is $T_S = 7.8$ μs, leading to a total storage time of $\tau_s = 1/\Delta + T_S = 12.8$ μs. From the trace with $\mu_{in} = 0$, we estimate an unconditional noise floor of $(2.0 \pm 0.3) \times 10^{-3}$ photons per pulse at the memory crystal. For $\mu_{in} = 1.15$, we measure a SNR $= 16.3 \pm 2.4$. The linear scaling of the echo SNR with respect to increasing μ_{in} is shown with blue circles in Fig. 2(b). Typical values of efficiencies are $\eta_{AFC} = (5.6 \pm 0.3)\%$ and $\eta_{SW} = (2.8 \pm 0.1)\%$, from which we deduce $\eta_T = (81.7 \pm 2.6)\%$ (assuming $\eta_C \sim 75\%$ [32]). A convenient figure of merit taking into account the noise and efficiency is given by the minimum μ_{in} necessary to detect a spin-wave echo with a SNR = 1, called μ_1. From the linear fit of the experimental data of Fig. 2(b), we find $\mu_1 = 0.069 \pm 0.002$. We then vary τ_s by changing T_S with $\mu_{in} = 1$, as shown in Fig. 2(c). The decay in the SNR is compatible with a spin inhomogeneous broadening of $\gamma_{in} = (26 \pm 1)$ kHz, similar to previous measurements with bright pulses [31,32]. We still observe a SNR $= 4.5 \pm 0.4$ for $T_S = 18.8$ μs ($\tau_s = 23.8$ μs).

We can estimate the contribution of the filter crystal in the suppression of the noise by preparing a wider transparency window. For a filter width of 14 MHz [squares in Fig. 2(b)] there is no filtering at the control frequency, and we observe an increase of the noise floor to $(2.3 \pm 0.6) \times 10^{-2}$ together with a slightly higher retrieval efficiency [$\eta_{SW} = (2.9 \pm 0.2)\%$], which results in μ_1 values up to about 1. When the filter crystal is bypassed, the noise floor rises to (0.23 ± 0.01), indicating that the inhomogeneously broadened absorption profile of Pr^{3+} also contributes to partially filter the noise [28]. Nonetheless, for this set of measurements, we were able to achieve a higher storage efficiency, i.e., $\eta_{SW} = (5.3 \pm 0.5)\%$, leading to a limited increase of μ_1 to about 4.

For applications in QIS, it is crucial that the optical memory preserve the coherence of the stored qubits. We take advantage of the intrinsic temporal multimodality of the AFC protocol to demonstrate the phase preservation in the spin-wave storage of time-bin qubits. This type of encoding is widely used in quantum communication as it is robust against decoherence in optical fibers [39]. The time-bin qubits are expressed as $|\psi_{in}\rangle = c_1|e\rangle + c_2 e^{i\Delta\alpha}|l\rangle$, where $|e\rangle$ ($|l\rangle$) represents a qubit in the early (late) time bin, $\Delta\alpha$ is their relative phase, and $c_1^2 + c_2^2 = 1$. In order to store time-bin qubits, the duration of the input pulses is reduced (from 430 to 260 ns), leading to a reduction of η_{SW} to about 2.2% and to an increase of μ_1 up to $\mu_{1p} = 0.11 \pm 0.01$. We start by evaluating the fidelity of the states $|e\rangle$ and $|l\rangle$, located at the poles of the Bloch sphere, F_e and F_l, by storing only the early and the late qubits. We obtain average fidelity values for the poles ranging from $F_{el} = 85\%$ to 98% for the photon number per qubit, μ_q, going from 0.6 to 5.9 [41]. We then store superposition states located on the equator of the Bloch sphere. We use the memory itself to analyze the retrieved qubits [33], applying two partial write pulses as depicted in Fig. 3(a). This method provides a convenient way of analyzing time-bin qubits, but has the drawback of reducing the storage efficiency. As a matter of fact, in order to insert two write pulses, their duration needs to be reduced, which decreases their efficiency. Figure 3(b) reports examples of interference fringes for $\mu_q = 1.5$. From sinusoidal fits, we obtain a raw mean visibility of $V_{+-} = (72.5 \pm 1.3)\%$. The fidelity of the process is calculated from the visibility, as $F = (1 + V)/2$ [39]. Finally, we obtain a total conditional fidelity per retrieved qubit $F_T = \frac{1}{3}F_{el} + \frac{2}{3}F_{+-}$, where F_{el} (F_{+-}) is the average fidelity over the poles (equator) basis. The obtained values are reported in Fig. 4 for different μ_q. We observe that the fidelity decreases with μ_q. To explain this behavior, we fit our data with a simple model taking into account the decrease of the SNR with μ_q and the reduced

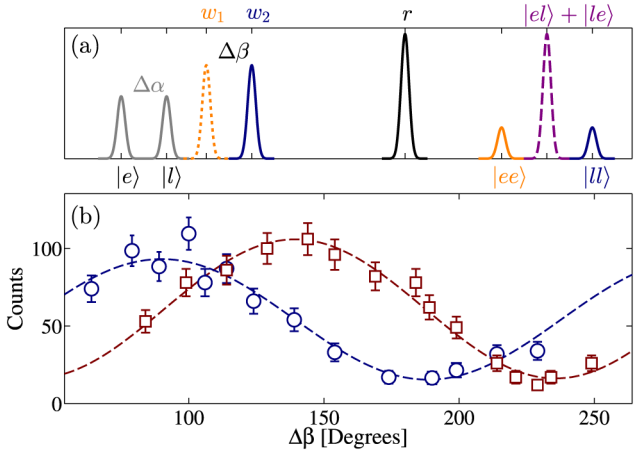

FIG. 3 (color online). (a) Pulse sequence to measure the time-bin qubit coherence. We apply two partial write pulses with a relative phase $\Delta\beta$ in order to split each pulse into two temporally separated echoes. If the delay between the time bins $|e\rangle$ and $|l\rangle$ is equal to the time difference between the two write pulses, we can overlap the late echo of the early bin, $|el\rangle$, with the early echo of the late bin, $|le\rangle$. The output of the memory (occurring after the single read pulse r) has three time bins, $\{|ee\rangle, |el\rangle + |le\rangle, |ll\rangle\}$. An interference will occur in the central time bin if the coherence is preserved. The input pulses, located at $|e\rangle$ and $|l\rangle$, have a relative phase difference of $\Delta\alpha$. (b) Interference fringes obtained integrating over the central output time bin (in this case $\Delta t_d = 0.5\ \mu$s) as a function of the relative phase difference $\Delta\beta$ for $\mu_q = 1.5$. Circles: $\Delta\alpha = 90°$, $V = (71.6 \pm 6.8)\%$. Squares: $\Delta\alpha = 135°$, $V = (73.4 \pm 3.5)\%$.

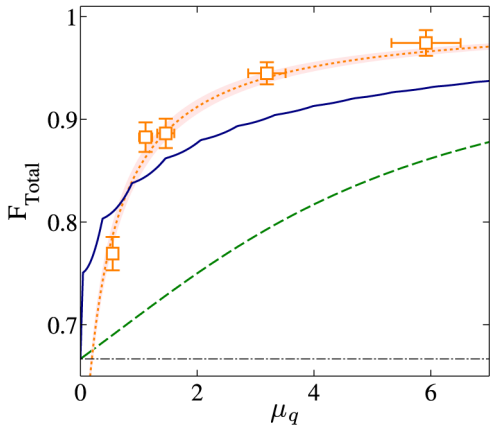

FIG. 4 (color online). Total fidelity versus input photon number per qubit, μ_q. The light orange squares are the data points with an error bar of 1 standard deviation. The orange dotted line is a fit to the data points using Eq. (5) in Ref. [41], with the corresponding shaded area being the 1 standard deviation of the error in this fit. The solid blue (dashed green) line is the classical limit obtained by a measure-and-prepare strategy for our memory efficiency of $\eta_{sw} = 2.2\%$ ($\eta_{sw} = 100\%$) when testing the memory with weak coherent states [25]. The dash-dotted line is the classical limit for testing the memory with a single-photon Fock state ($F = 2/3$).

efficiency due to the double write protocol [41]. The good agreement between the simple model and the data provides evidence that the decrease of fidelity is only due to the noise created by the control pulses, and not to a loss of coherence.

In order to infer the quantum nature of our memory, the total fidelity is compared with the highest fidelity achievable with a measure-and-prepare approach (solid curve in Fig. 4), taking into account the Poissonian statistics of the input states and the finite memory efficiency (2.2%) [4,11,25]. Using this criteria, the experimental data are higher than the limit for a classical memory by more than 1 standard deviation for most μ_q investigated. With the raw data, the memory is in the quantum regime for $\mu_q > 0.96$. When correcting for the loss of efficiency in the analysis (which could be achieved by analyzing the qubits with an external interferometer), the model predicts that the quantum regime would be reached for $\mu_q > 0.25$ (see Ref. [41]).

The very low noise probability and the ability to obtain $\mu_1 \ll 1$ opens prospects for the spin-wave storage of single photons, as required for many applications in QIS. In that case, the probability to have a photon before the memory (i.e., including all optical loss between the source and memory) needs to be higher than μ_1 to enter the quantum regime. In the current experiment, the storage efficiency is limited by the available comb optical depth in our 3 mm long crystal, by the limited transfer efficiency [$\eta_T^2 = (67 \pm 4)\%$], and by technical issues (cryostat vibrations, laser linewidth, see Ref. [41]). Note that much higher efficiencies (for storage in the excited state) have been obtained in $Pr^{3+}:Y_2SiO_5$ using a longer crystal (69%) [16] or impedance matched cavities (58%) [49]. Longer storage times can also be achieved with dynamical decoupling techniques to counteract decoherence in the spin state [34,35,50,51].

In conclusion, we demonstrated the spin-wave storage and on-demand retrieval of weak coherent states at the single-photon level in a solid state memory based on a $Pr^{3+}:Y_2SiO_5$ crystal. This is the first demonstration that solid state spin-wave optical memories can operate in the quantum regime, overcoming a strong limitation for AFC QMs. We achieved a SNR higher than 10 for single-photon level input pulses, high enough to enable the storage of single photons. Finally, we confirmed the quantum nature of our memory by storing time-bin qubits encoded in weak coherent states and demonstrating conditional fidelities for the retrieved qubits higher than what is possible with classical memories. Our device thus represents the first spin-wave memory for photonic time-bin qubits. These results open the door for long-lived storage and on-demand read-out of nonclassical light states in solid state devices and represent an important step in view of using solid state quantum memories in scalable quantum architectures.

We acknowledge financial support by the ERC starting grant QuLIMA, by the Spanish Ministry of Economy and Competitiveness (MINECO) and the Fondo Europeo de Desarrollo Regional (FEDER) through Grant No. FIS2012-37569, by the European project CHIST-ERA QScale, and by the People Programme (Marie Curie Actions) of the EU FP7 under REA Grant Agreement No. 287252.

Note added in proof.—A related experiment demonstrating single-photon-level spin-wave storage in a Europium-doped crystal has been performed in parallel [52].

*Present address: Department of Physics, Clarendon Laboratory, University of Oxford, Oxford OX1 3PU, United Kingdom.
†margherita.mazzera@icfo.es

[1] L.-M. Duan, M. D. Lukin, J. I. Cirac, and P. Zoller, Nature (London) **414**, 413 (2001).
[2] N. Sangouard, C. Simon, H. de Riedmatten, and N. Gisin, Rev. Mod. Phys. **83**, 33 (2011).
[3] E. Knill, R. Laflamme, and G. J. Milburn, Nature (London) **409**, 46 (2001).
[4] H. P. Specht, C. Nölleke, A. Reiserer, M. Uphoff, E. Figueroa, S. Ritter, and G. Rempe, Nature (London) **473**, 190 (2011).
[5] C. W. Chou, H. de Riedmatten, D. Felinto, S. V. Polyakov, S. J. van Enk, and H. J. Kimble, Nature (London) **438**, 828 (2005).
[6] T. Chanelière, D. N. Matsukevich, S. D. Jenkins, S.-Y. Lan, T. A. B. Kennedy, and A. Kuzmich, Nature (London) **438**, 833 (2005).
[7] K. S. Choi, H. Deng, J. Laurat, and H. J. Kimble, Nature (London) **452**, 67 (2008).
[8] H. Zhang *et al.*, Nat. Photonics **5**, 628 (2011).
[9] M. Lettner, M. Mücke, S. Riedl, C. Vo, C. Hahn, S. Baur, J. Bochmann, S. Ritter, S. Dürr, and G. Rempe, Phys. Rev. Lett. **106**, 210503 (2011).
[10] S. Riedl, M. Lettner, C. Vo, S. Baur, G. Rempe, and S. Dürr, Phys. Rev. A **85**, 022318 (2012).
[11] A. Nicolas, L. Veissier, L. Giner, E. Giacobino, D. Maxein, and J. Laurat, Nat. Photonics **8**, 234 (2014).
[12] B. Julsgaard, J. Sherson, J. Ignacio Cirac, J. Fiurášek, and E. S. Polzik, Nature (London) **432**, 482 (2004).
[13] M. Hosseini, G. Campbell, B. M. Sparkes, P. K. Lam, and B. C. Buchler, Nat. Phys. **7**, 794 (2011).
[14] M. Sprague, P. S. Michelberger, T. F. M. Champion, D. G. England, J. Nunn, X.-M. Jin, W. S. Kolthammer, A. Abdolvand, P. St. J. Russell, and I. A. Walmsley, Nat. Photonics **8**, 287 (2014).
[15] H. de Riedmatten, M. Afzelius, M. U. Staudt, C. Simon, and N. Gisin, Nature (London) **456**, 773 (2008).
[16] M. P. Hedges, J. J. Longdell, Y. Li, and M. J. Sellars, Nature (London) **465**, 1052 (2010).
[17] C. Clausen, I. Usmani, F. Bussières, N. Sangouard, M. Afzelius, H. de Riedmatten, and N. Gisin, Nature (London) **469**, 508 (2011).
[18] E. Saglamyurek, N. Sinclair, J. Jin, J. A. Slater, D. Oblak, F. Bussières, M. George, R. Ricken, W. Sohler, and W. Tittel, Nature (London) **469**, 512 (2011).
[19] E. Togan *et al.*, Nature (London) **466**, 730 (2010).
[20] H. Bernien *et al.*, Nature (London) **497**, 86 (2013).
[21] D. G. England, K. A. G. Fisher, J.-P. W. MacLean, P. J. Bustard, R. Lausten, K. J. Resch, and B. J. Sussman, Phys. Rev. Lett. **114**, 053602 (2015).
[22] R. M. Macfarlane, J. Lumin. **100**, 1 (2002).
[23] M. Afzelius, C. Simon, H. de Riedmatten, and N. Gisin, Phys. Rev. A **79**, 052329 (2009).
[24] N. Sinclair *et al.*, Phys. Rev. Lett. **113**, 053603 (2014).
[25] M. Gündoğan, P. M. Ledingham, A. Almasi, M. Cristiani, and H. de Riedmatten, Phys. Rev. Lett. **108**, 190504 (2012).
[26] C. Clausen, F. Bussières, M. Afzelius, and N. Gisin, Phys. Rev. Lett. **108**, 190503 (2012).
[27] Z.-Q. Zhou, W. B. Lin, M. Yang, C. F. Li, and G. C. Guo, Phys. Rev. Lett. **108**, 190505 (2012).
[28] D. Rieländer, K. Kutluer, P. M. Ledingham, M. Gündoğan, J. Fekete, M. Mazzera, and H. de Riedmatten, Phys. Rev. Lett. **112**, 040504 (2014).
[29] I. Usmani, C. Clausen, F. Bussières, N. Sangouard, M. Afzelius, and N. Gisin, Nat. Photonics **6**, 234 (2012).
[30] F. Bussières *et al.*, Nat. Photonics **8**, 775 (2014).
[31] M. Afzelius *et al.*, Phys. Rev. Lett. **104**, 040503 (2010).
[32] M. Gündoğan, M. Mazzera, P. M. Ledingham, M. Cristiani, and H. de Riedmatten, New J. Phys. **15**, 045012 (2013).
[33] N. Timoney, I. Usmani, P. Jobez, M. Afzelius, and N. Gisin, Phys. Rev. A **88**, 022324 (2013).
[34] J. J. Longdell, E. Fraval, M. J. Sellars, and N. B. Manson, Phys. Rev. Lett. **95**, 063601 (2005).
[35] G. Heinze, C. Hubrich, and T. Halfmann, Phys. Rev. Lett. **111**, 033601 (2013).
[36] H. Zhang, M. Sabooni, L. Rippe, C. Kim, S. Kröll, L. V. Wang, and P. R. Hemmer, Appl. Phys. Lett. **100**, 131102 (2012).
[37] S. E. Beavan, M. P. Hedges, and M. J. Sellars, Phys. Rev. Lett. **109**, 093603 (2012).
[38] S. E. Beavan, E. A. Goldschmidt, and M. J. Sellars, J. Opt. Soc. Am. B **30**, 1173 (2013).
[39] I. Marcikic, H. de Riedmatten, W. Tittel, H. Zbinden, and N. Gisin, Nature (London) **421**, 509 (2003).
[40] P. Humphreys, B. J. Metcalf, J. B. Spring, M. Moore, X.-M. Jin, M. Barbieri, W. Steven Kolthammer, and I. A. Walmsley, Phys. Rev. Lett. **111**, 150501 (2013).
[41] See Supplemental Material at http://link.aps.org/supplemental/10.1103/PhysRevLett.114.230501, for details on the memory preparation, noise and filter characterization and modelling of the storage and recall fidelity, which includes Refs. [42–44].
[42] O. Guillot-Noël, Ph. Goldner, Y. Le Du, P. Loiseau, B. Julsgaard, L. Rippe, and S. Kröll, Phys. Rev. B **75**, 205110 (2007).
[43] M. Bonarota, J. Ruggiero, J.-L. Le Gouët, and T. Chanelière, Phys. Rev. A **81**, 033803 (2010).
[44] D. L. McAuslan, J. J. Longdell, and M. J. Sellars, Phys. Rev. A **80**, 062307 (2009).
[45] P. S. Michelberger *et al.*, New J. Phys. **17**, 043006 (2015).
[46] N. Maring, K. Kutluer, J. Cohen, M. Cristiani, M. Mazzera, P. M. Ledingham, and H. de Riedmatten, New J. Phys. **16**, 113021 (2014).
[47] M. Nilsson, L. Rippe, S. Kroll, R. Klieber, and D. Suter, Phys. Rev. B **70**, 214116 (2004).
[48] O. Guillot-Noël, Ph. Goldner, F. Beaudoux, Y. Le Du, J. Lejay, A. Amari, A. Walther, L. Rippe, and S. Kröll, Phys. Rev. B **79**, 155119 (2009).
[49] M. Sabooni, Q. Li, S. Kröll, and L. Rippe, Phys. Rev. Lett. **110**, 133604 (2013).
[50] M. F. Pascual-Winter, R.-C. Tongning, T. Chanelière, and J.-L. Le Gouët, Phys. Rev. B **86**, 184301 (2012).
[51] M. Lovric, D. Suter, A. Ferrier, and P. Goldner, Phys. Rev. Lett. **111**, 020503 (2013).
[52] P. Jobez, C. Laplane, N. Timoney, N. Gisin, A. Ferrier, P. Goldner, and M. Afzelius, following Letter, Phys. Rev. Lett. **114**, 230502 (2015).